Supporting Information

Directional coalescence growth of ultralong $Au_{93}Pt_7$ alloy nanowire and its superior electrocatalytic performance for ethanol oxidation

Qi-Min Gan, Li Tao, Lin-Nan Zhou, Xiao-Ting Zhang, Shuangyin Wang, * Yong-Jun Li*

State Key Laboratory of Chemo/Biosensing and Chemometrics, School of Chemistry and Chemical Engineering, Hunan University, Changsha 410082, China.

Experimental Section

Materials. Hexachloroplatinic acid hexahydrate ($H_2PtCl_6.6H_2O$, 37 wt%), chloride tetrahydrate ($HAuCl_4 \cdot 4H_2O$, 47.8 wt%), *L*-ascorbic acid (AA, 99.7 wt%), acetone (CH_3COCH_3) and ethanol (C_2H_5OH) were supplied by Sinopharm Chemical Reagent Co. Ltd. (China). Commercial Pt/C (Pt, 20 wt%) was obtained from Johnson Matthey Company, polyvinylpyrrolidone (PVP, M_w = 29000) was purchased from Sigma-Aldrich. Cetyltrimethylammonium bromide (CTAB) was purchased from Ruibio (Gemany). All chemicals were used as received. Milli-Q ultrapure water (18.2 MΩ·cm) was used in all experiments.

Synthesis of $Au_{93}Pt_7$ alloy nanowires. Typically, 0.28 mL of 0.4 mol/L AA was quickly injected into 200 mL of an aqueous solution containing 5.4 mmol/L CTAB, 5.4 mmol/L PVP, 0.0972 mmol/L $HAuCl_4$, and 0.0972 mmol/L H_2PtCl_6 under sonication. The color of the solution turned from orange to light yellow in 30 s due to the reduction of Au^{3+} to Au^+ (Au^+ ions are colorless and the color comes from H_2PtCl_6 precursors). Subsequently, the mixed solution was held silently at 30 ^oC for 6 h for the formation of Au nanowires. AuPt nanowires were collected by centrifugation, washed once with acetone and two times with ethanol, and dried at 60 ^oC for characterization and performance test. Inductively coupled plasma-optical emission spectroscopy (ICP-OES) analysis indicates that the average atomic ratio of Au to Pt is 93:7. Thus, as-prepared AuPt nanowire sample was called $Au_{93}Pt_7$.

Fabrication of catalytic electrode. Glassy carbon (GC) disk (diameter, 3 mm) was used as an electrode substrate to support catalyst particles after polished successively

with 1.0 μm-, 0.3 μm- and 0.05 μm-alumina slurry, and ultrasonically rinsed twice with water and ethanol. A certain amount of commercial Pt/C and as-prepared AuPt nanowire catalyst ink was prepared by dispersing the drying powders into ultrapure water, the final concentration of which is 2 mg/mL, respectively. 5 μL of as-prepared catalyst ink was spread on GC surface and dried in the air at room temperature. Subsequently, 3 μL of 5 wt % Nafion ethanol solution was covered the surface of catalyst for solidification.

The procedure of electrochemical experiments. All electrochemical experiments were conducted on a conventional three-electrode configuration at room temperature. A saturated calomel electrode (SCE) and a platinum wire were used as the reference electrode and the counter electrode, respectively. All potentials mentioned below refer to SCE unless otherwise specified. GC modified with AuPt alloy nanowires or Pt/C catalyst served as the working electrode. Ethanol electrooxidation were carried out in 50 mL of 1.0 mol/L NaOH solution containing 1.0 mol/L CH_3CH_2OH at 50 $mV \cdot s^{-1}$ between –0.90 and 0.6 V. Before that, the working electrode was further cleaned by cycling between –0.2 and 1.4 V at 50 $mV \cdot s^{-1}$ in 0.5 mol/L H_2SO_4 solution until the pattern of the cycle voltammogram did not change, and N_2 was bubbled through NaOH + CH_3CH_2OH solution for 15 min to eliminate dissolved O_2.

Instruments and characterization. All electrochemical experiments were performed on a CHI 660D workstation (Chenhua, Shanghai). Transmission electron microscopy (TEM), high resolution transmission electron microscopy (HRTEM), and energy dispersive X-ray (EDX) spectra were obtained on a JEM-3010 microscope (JEOL, Japan) with an Oxford INCA detector operating at 300 kV. The compositions of AuPt nanowires were determined through an inductively coupled plasma-optical emission spectroscopy (ICP-OES) (Optimal 5300DV spectrometer, PerkinElmer Inc.). Scanning electron microscopy (SEM) analysis was performed on a HitachiS-4800. Elemental mapping analysis was performed in the STEM mode on a FEI Tecnai G2 F20 Field Emission TEM. X-ray photoelectron spectroscopy (XPS) was conducted on a K-Alpha 1063 X-ray photoelectron spectrometer (Thermo Fisher Scientific) with Al Ka X-rays as the excitation source. X-ray diffraction (XRD) measurement was

performed on a θ-2θ X-ray diffraction Shimadzu XRD-6100.

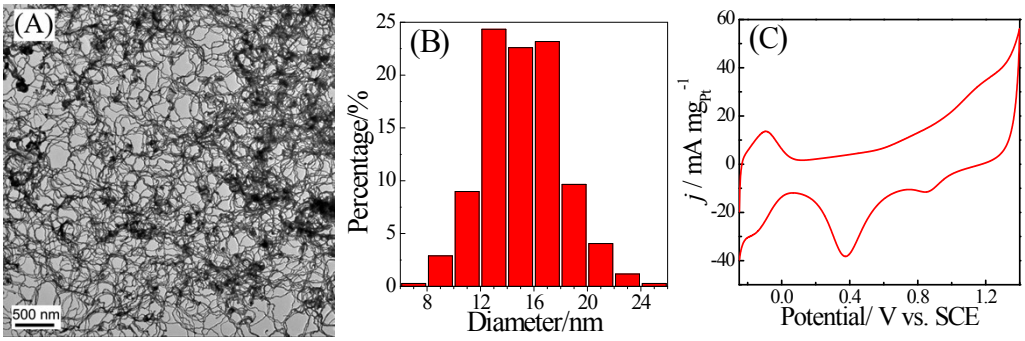

Fig. S1 TEM image (A), histogram of $Au_{93}Pt_7$ nanowire diameters (B) and cyclic voltammogram (C) of $Au_{93}Pt_7$ nanowires in 0.5 mol/L H_2SO_4 at a scan rate of 50 mV/s.

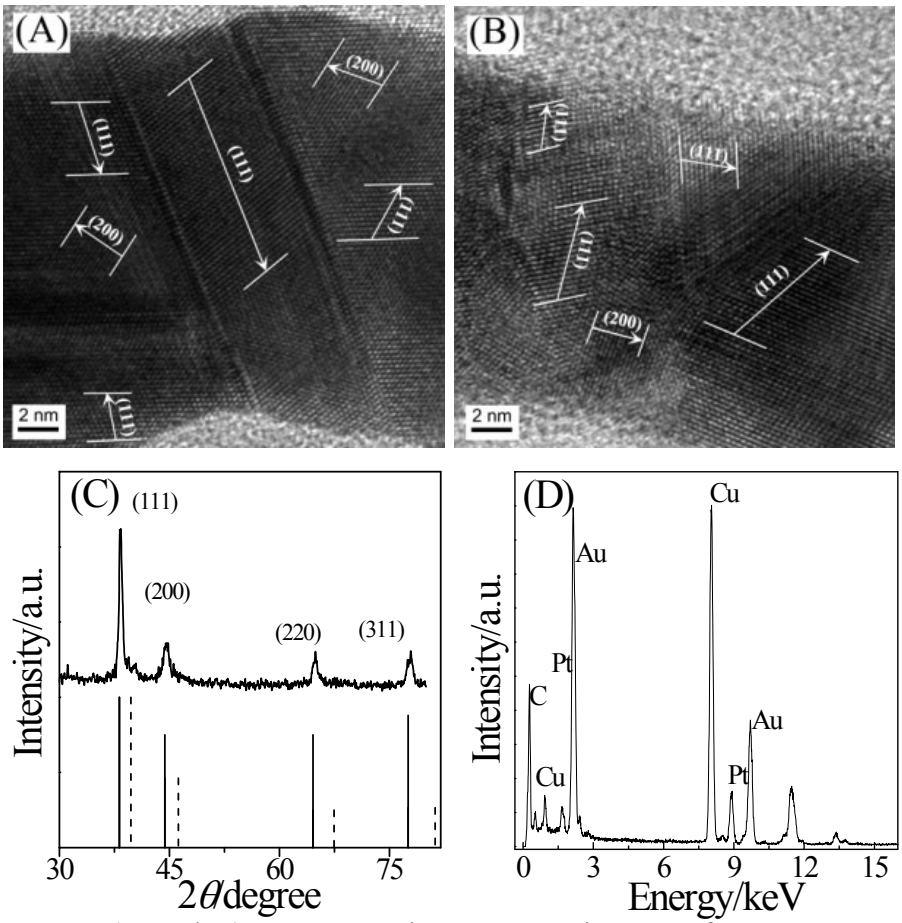

Fig. S2 (A and B) Representative HRTEM images of $Au_{93}Pt_7$ nanowires. (C) XRD pattern of $Au_{93}Pt_7$ nanowires. Solid lines and dash lines perpendicular to the horizontal axis represent diffraction peak positions of face-centered cubic Au (JCPDS 04-0784) and Pt (JCPDS 70-2431), respectively. (D) EDX spectrum of $Au_{93}Pt_7$ nanowires.

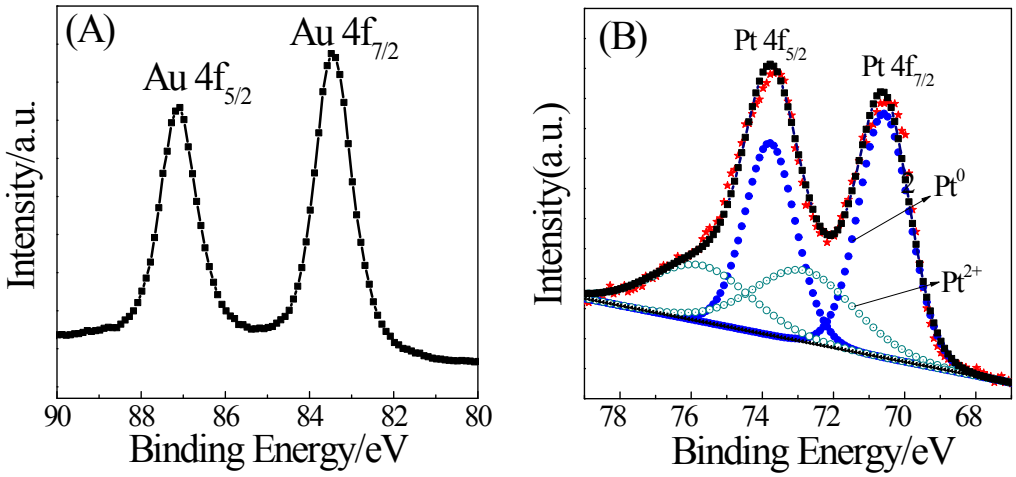

Fig. S3 Au 4f (A) and Pt 4f (B) XPS spectroscopy of $Au_{93}Pt_7$ nanowires. In the case of Pt 4f, Black curves are the original patterns; red curves are the simulated patterns by the curves of the deconveluted components of Pt^0 (blue) and Pt^{2+} (dark cyan) species.

To further resolve the surface composition and chemical state of the as-prepared bimetallic $Au_{93}Pt_7$ nanowires, X-ray photoelectron spectroscopy (XPS) was employed to detect Au 4f and Pt 4f binding energy. The energy band of Au $4f_{7/2}$ or $4f_{5/2}$ (Fig. S3A) is a symmetrical peak, and the relative intensity ratio of Au $4f_{7/2}$ to $4f_{5/2}$ is close to the theoretical value of 4:3,[1] indicating that Au element exists in metallic state. The energy band of Au $4f_{7/2}$ and $4f_{5/2}$ centers at 87.1 eV and 83.5 eV, slightly shifting to the low-energy direction in comparison with pure Au ($4f_{5/2}$, 87.6 eV; $4f_{7/2}$, 83.9 eV),[2] which may be attributed to the perturbed electronic interaction between Pt and Au atomic orbit, i.e. the charge transfer of Pt to Au due to the difference of the electronegativity of Au (2.31) and Pt (2.13),[2] which has been observed in Au-Pt heterogeneous junction.[3] In the case of Pt, the energy band of Pt $4f_{7/2}$ or $4f_{5/2}$ (Fig. S3B) is a symmetrical peak, indicating that Pt in $Au_{93}Pt_7$ nanowires is not completely in metallic state, as demonstrated by Zhou et al.[4] that Pt in AuPt alloy is more inclined to be oxidized than Au. By the deconvolution of Pt XPS pattern, two components were determined: one located at 75.73 and 73.78 eV (dark cyan curves in Fig. S3B), the other at 72.83 and 70.58 eV (blue curves in Fig. S3B). The former belongs to Pt^{2+} ions; the latter belongs to metallic Pt^0, but are slightly higher than the binding

energies of pure Pt $4f_{5/2}$(74.5 eV) and $4f_{7/2}$ (71.2 eV),[2] respectively, which may be caused by the alloying of Pt with Au and the coexistence of Pt^{2+} ions. Metallic Pt^0 is the predominant species, ~64 % of the total number of Pt atoms. XPS surface analysis also indicates the Au:Pt atomic ratio is ~21:79, further confirming the richness of Pt on the surface of $Au_{93}Pt_7$, consistent with the result of Fig. 1D and S1C.

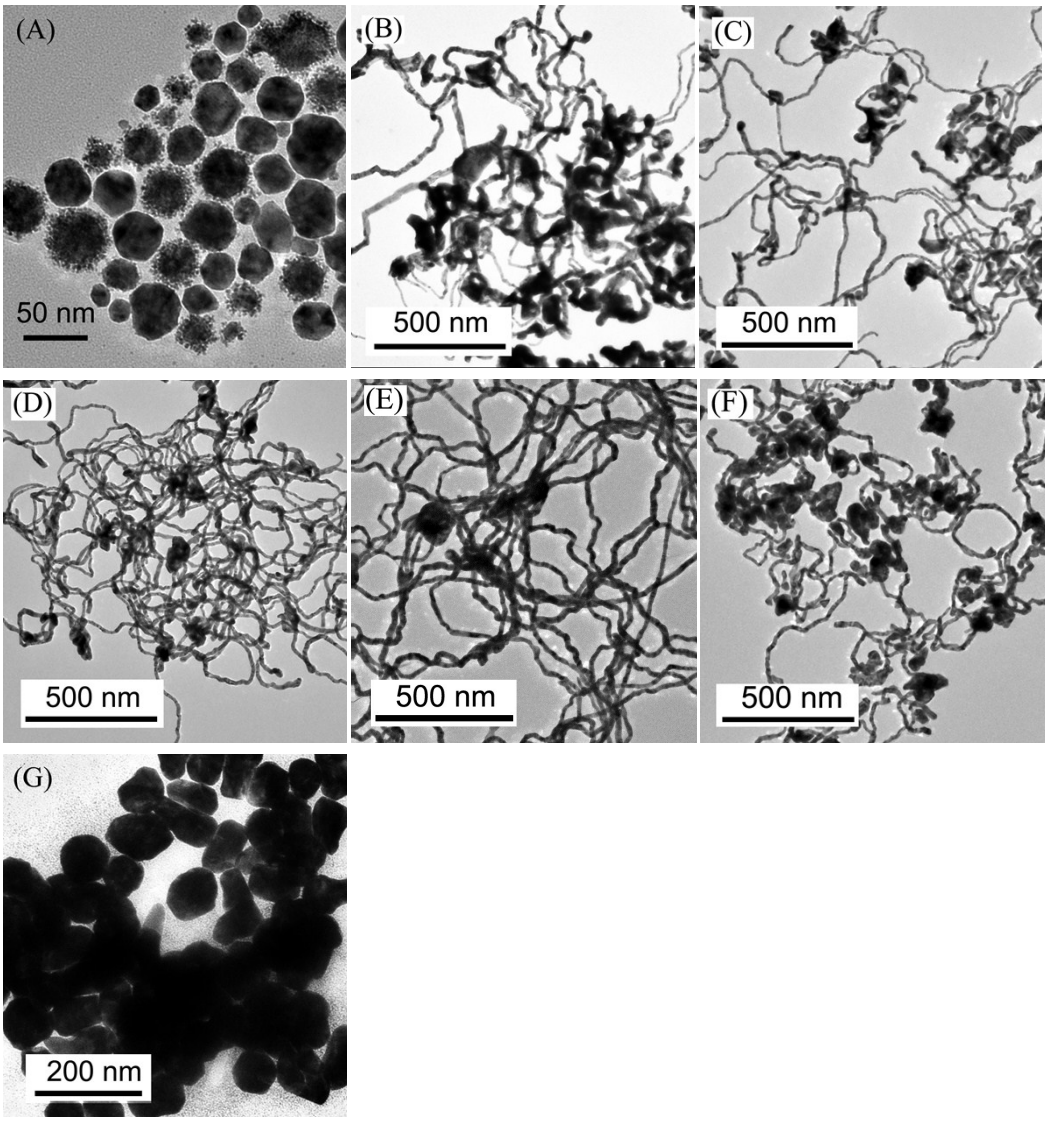

Fig. S4 TEM images of the samples obtained by adjusting the PVP:CTAB molar ratio: (A) PVP without CTAB, (B) 1:0.25, (C) 1:0.5, (D) 1:0.75, (E) 1:1.5, (F) 1:2, and (G) CTAB without PVP.

To understand the growth mechanism of $Au_{93}Pt_7$ nanowires, the effect of the PVP:CTAB and $HAuCl_4$:H_2PtCl_6 molar ratios were discussed, respectively. Fig. S4 show TEM images of the samples prepared by adjusting the PVP:CTAB molar ratios

with other conditions remaining the same as the synthesis of $Au_{93}Pt_7$ nanowires. When only PVP was used as the surfactant without CTAB, the resulting samples contains multi-morphological nanoparticles (Fig. S4A), and some particles have Au/Pt core/shell structures: tiny Pt nanoparticles decorate on the surface of Au nanoparticle, indicating that $AuCl_4^-$ species are firstly reduced to form Au nanoparticles, on the surface of which tiny Pt nanoparticles, subsequently, grow. However, when CTAB was introduced as another surfactant, the morphologies of as-prepared samples completely changes. When the amount of CTAB gradually increases, i.e. the PVP:CTAB molar ratio varies from 1:0.25 to 1:0.5 (Fig. S4B and C), nanowires appears companied by some irregular nanoparticles and the increase of CTAB amount benefits the yield and quality of nanowires. Over the range of the PVP:CTAB molar ratios from 1:0.75 to 1:1.5, as-prepared samples are mainly composed of nanowires (Fig. S4D and S4E, and Fig. 1). Continually increasing the amount of CTAB does not have a positive role in the growth of high-quality nanowires: the mixture of nanoparticles and short nanowires were observed again (Fig. S4F). If CTAB was used as a single surfactant, the sample mainly consists of multiple-shaped particles (Fig. S4G). Thus, the formation of AuPt nanowire cannot be achieved when the single PVP or CTAB is used; high-quality AuPt nanowires depends on the PVP:CTAB molar ratios and can be well formed over the range of the PVP:CTAB molar ratio from 1:0.75 to 1:1.5. Interestingly, ICP-OES analysis indicates that the Au:Pt atomic ratios of these nanowires in Fig. S4B-F are similar and changes over the narrow range of 91:9 to 95:5, and the Pt content has a tendency of reduction with the increase of CTAB amount.

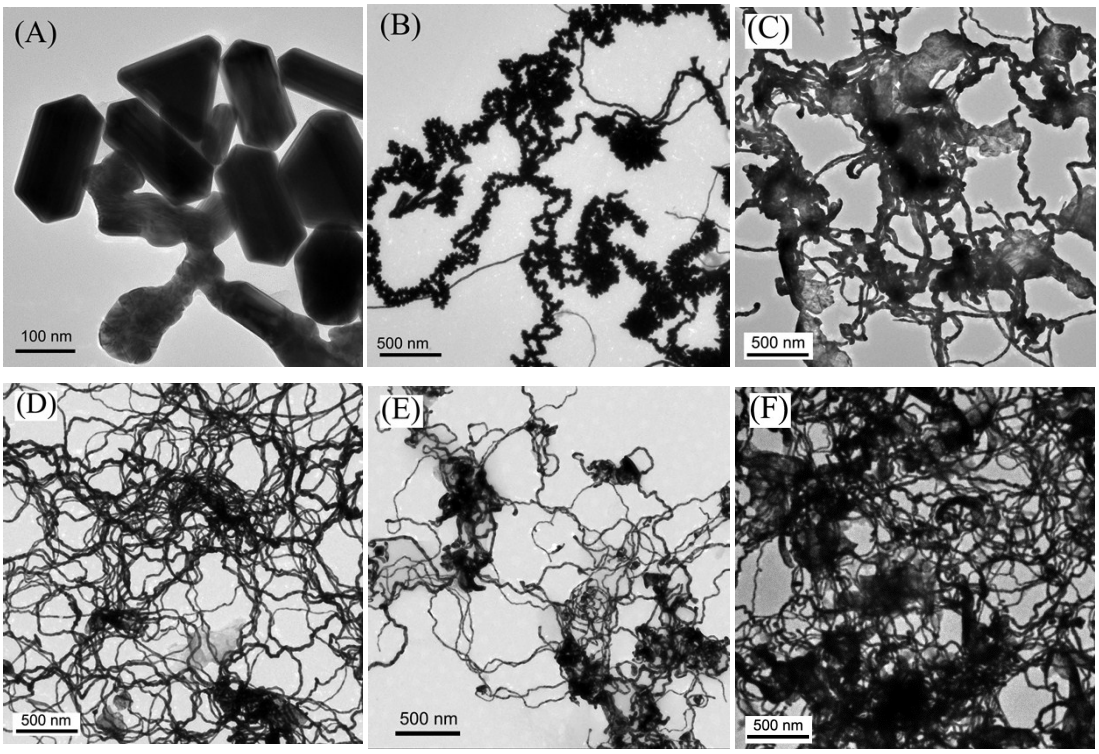

Fig. S5 TEM images of samples prepared by controlling the concentration ratios of $HAuCl_4$:H_2PtCl_6: (A) $HAuCl_4$ without H_2PtCl_6, (B) 1:0.25, (C) 1:0.5, (D) 1:0.75, (E) 1:1.25, and (F) 1:2.

Under the appropriate PVP:CTAB molar ratios (over the range from 1:0.75 to 1:1.5), can the Au:Pt atomic ratio of AuPt nanowire be adjusted by controlling the molar ratio of Au to Pt precursors? Is the formation of AuPt nanowire dependent on the molar ratios of Au to Pt precursors? To address these issues, the synthesis was carried out with different $HAuCl_4$:H_2PtCl_6 molar ratios. When single $HAuCl_4$ precursors were used, multi-shaped Au nanoparticles were formed (Fig. S5A), where some rod-like shapes was also observed, which may be directly related to the guidance role of CTAB.[5] When H_2PtCl_6 precursors were introduced and the $HAuCl_4$:H_2PtCl_6 molar ratio is 1:0.25, the product is necklace-like one-dimensional structure (Fig. S5B), completely different from the case of single $HAuCl_4$ precursors, indicating that introduction of H_2PtCl_6 can bring about a morphology change. When $HAuCl_4$:H_2PtCl_6 = 1:0.5, the proportion of smooth nanowires increase along with the coexistence of many amorphous nanosheets (Fig. S5C). When the $HAuCl_4$:H_2PtCl_6 molar ratio increases from 1:0.5 to 1:0.75, high-quality nanowires were obtained and

a majority of amorphous nanosheets disappear (Fig. S5D). Over the range of the $HAuCl_4$:H_2PtCl_6 molar ratios from 1:0.75 to 1:1, the yield and quality of nanowires are the highest (Fig. S5D and Fig. 1). When continually increasing the amount of Pt precursor, a lot of coexisted amorphous nanosheets appear again and increase over the range of the $HAuCl_4$:H_2PtCl_6 molar ratios from 1:1.25 to 1:2 (Fig. S5E and F). Although the morphologies of as-prepared samples undergo a distinct evolution with different $HAuCl_4$:H_2PtCl_6 molar ratios, ICP-OES analysis revealed that the Au:Pt atomic ratios of AuPt nanowires obtained over the range of $HAuCl_4$:H_2PtCl_6 molar ratios from 1:0.25 to 1:2 are close to 93:7, completely independent of the molar ratio of $HAuCl_4$ to H_2PtCl_6 precursors. Thus, the Au:Pt atomic ratio of AuPt nanowires, in our case, cannot be adjusted by controlling the $HAuCl_4$:H_2PtCl_6 molar ratios.

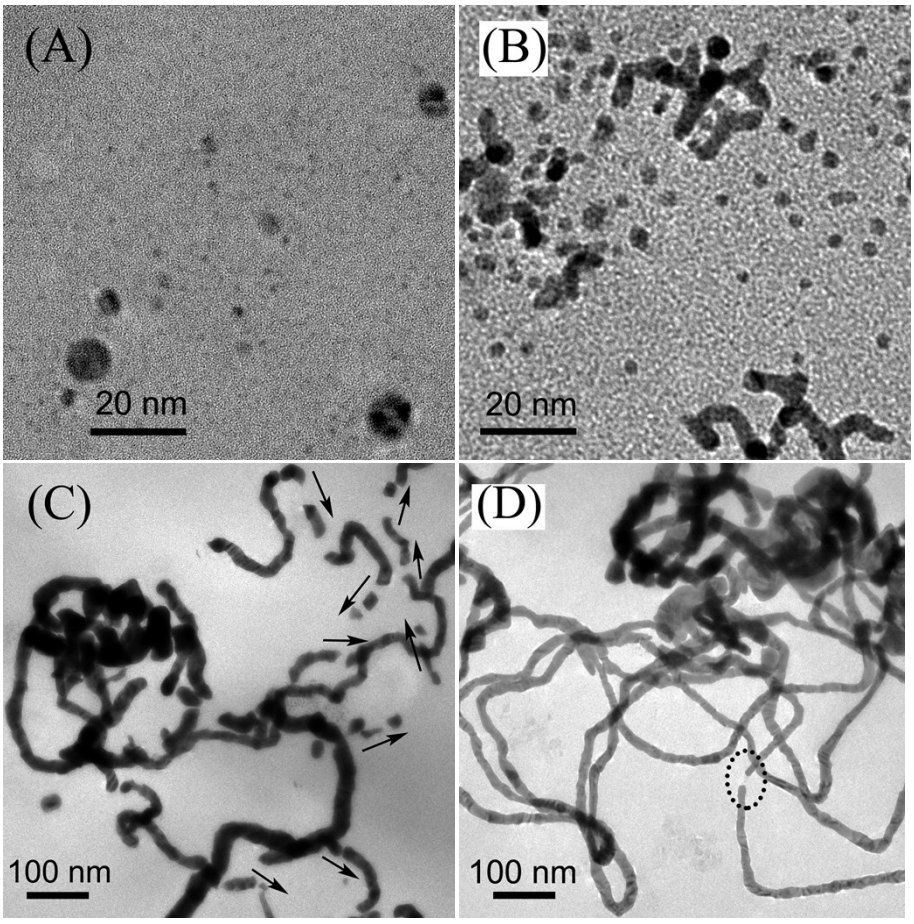

Fig. S6 TEM images of the different growth stage of $Au_{93}Pt_7$ nanowires: (A) 30 min, (B) 45 min, (C) 72 min, and (D) 130 min.

Fig. S6 shows TEM images of $Au_{93}Pt_7$ nanowires at different growth stages. After 30 min, plenty of tiny particles were observed accompanied by a few ~10-nm

nanoparticles (Fig. S6A). At 45 min, many ~3-nm nanoparticles appear and their coalescence results in the appearance of rod-like structures decorated with dentrities (Fig. S6B). At 72 min, short embryonic nanowires have been formed (Fig. S6C) and those short nanowires have a tendency to be joined end to end into long nanowires, as marked with arrows. At 130 min, many long nanowires have been formed, and the end-to-end connection also occurs between long nanowires, as marked with the dot circle in Fig. S6D. At 360 min, ultralong nanowires were produced (Fig. 1) without spherical and rod-like particles. The morphologies mentioned above represent the dominant products at different reaction time because the two morphologies in Fig. S6B and C were also observed at 130, 140, 160 and 190 min.

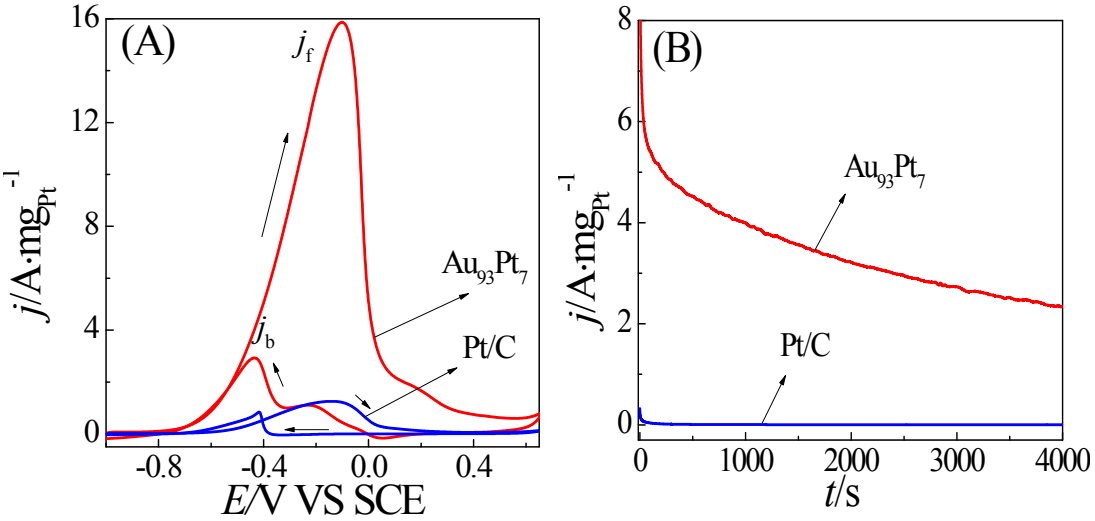

Fig. S7 (A) Voltammograms of $Au_{93}Pt_7$ and commercial Pt/C in 1.0 mol L^{-1} NaOH containing 1.0 mol L^{-1} C_2H_5OH at a scan rate of 50 mV/s. (B) Amperometric current-time curves of $Au_{93}Pt_7$ nanowires and commercial Pt/C at –0.3 V in 1.0 mol L^{-1} NaOH containing 1.0 mol L^{-1} C_2H_5OH.

Table S1 Summary of mass activities of Pt-based catalysts for ethanol electrooxidation in basic solution

Catalyst	Mass activity	Reference
$Au_{93}Pt_7$ alloy nanowire	~15.9 Amg^{-1}	This work
Au/Pd core/shell decorated with Pt shell	0.46 Amg^{-1}_{Pd+Pt}	6
PtAu alloy nanoflower	0.95 A mg^{-1}	7
PtPd alloy	1.49 A mg^{-1}_{PtPd}	8
concave Au/Pt core/shell nanocube	1.04 A mg^{-1}_{Pt}	9
$Ni_{40}Au_{33}Pt_{27}$ alloy nanoparticle	~4.94 A mg^{-1}_{Pt}	10
PtSnRh wavy nanowire	0.99 A mg^{-1}_{Pt}	11
porous Pt-PbO_x	~4.2 A mg^{-1}_{Pt}	12
Pd–Pt alloy	1.07A mg^{-1}_{PdPt}	13
$Au_{17}Pt_{24}Pd_{59}$ alloy nanowire	~3.2 A mg^{-1}_{metal}	14
Pt–Au nanodimer	~9.2 Amg^{-1}_{Pt}	15
Pt–Sn composite	0.285 Amg^{-1}_{Pt}	16
PtPd alloy nanoparticle	5.16 Amg^{-1}_{metal}	17
PtPb nanoparticle	4.5 Amg^{-1}_{Pt}	18
Pt and Pd quasi-monolayer on Au surface	~9.0 Amg^{-1}_{metal}	19

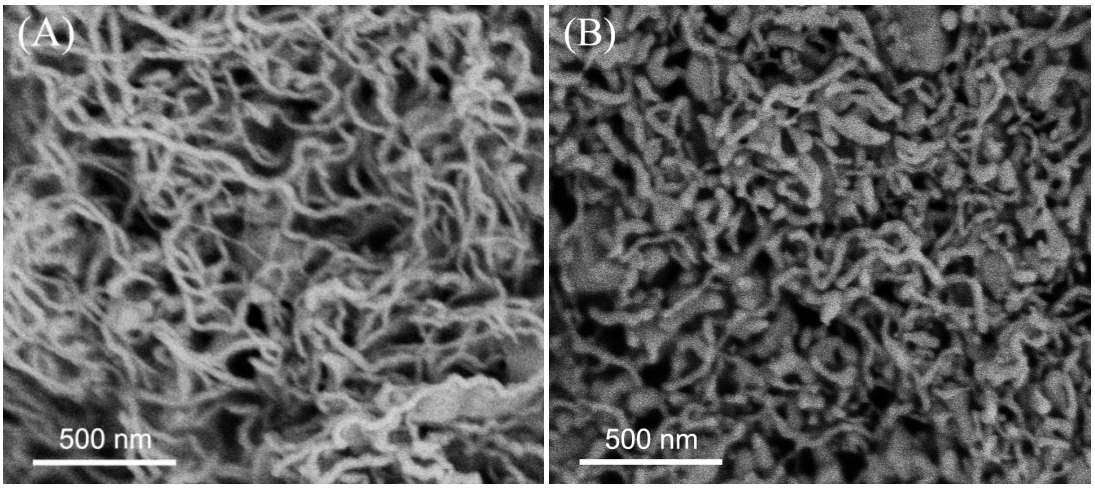

Fig. S8 SEM images of $Au_{93}Pt_7$ nanowires coated on the surface of glassy carbon before (A) and after (B) cycling for 16.5 h at 50 mV/s between −1.0 V and 0.65 V with the cyclic voltammetric technique in 1.0 mol L^{-1} NaOH + 1.0 mol L^{-1} C_2H_5OH.

Before electrooxidizing ethanol, the morphology of $Au_{93}Pt_7$ ANWs (Fig. S8A) is completely the same as that shown in Fig. 1B. After a long-term electroxidation (16.5 h), ultralong nanowires break into short ones (Fig. S8B), which may be responsible for the MA decay of $Au_{93}Pt_7$ ANWs rather than the surface poisoning.

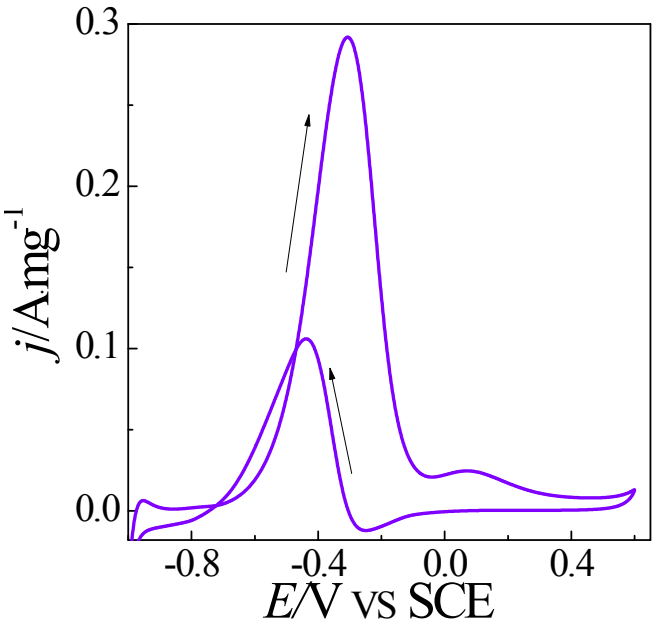

Fig. S9 Cyclic voltammogram of Au nanoparticles (Fig. S5A) in 1.0 mol L^{-1} NaOH containing 1.0 mol L^{-1} C_2H_5OH at a scan rate of 50 mV/s.

References

1. G. Selvarani, S. V. Selvaganesh, S. Krishnamurthy, G. V. M. Kiruthika, P. Sridhar,

S. Pitchumani and A. K. Shukla, *J. Phys. Chem. C*, 2009, **113**, 7461.
2. D. R. Lide, CRC Handbook of Chemistry and Physics, Taylor and Francis, Boca Raton, FL, 2007.
3. X. Teng, W. Han, Q. Wang, L. Li, A. I. Frenkel and J. C. Yang, *J. Phys. Chem. C*, 2008, **112**, 14696.
4. W. Zhou, M. Li, L. Zhang and S. H. Chan, *Electrochim. Acta*, 2014, **123**, 233.
5. N. R. Jana, L. Gearheart and C. J. Murphy, *J. Phys. Chem. B*, 2001, **105**, 4065.
6. G.-R. Zhang, J. Wu and B.-Q. Xu, *J. Phys. Chem. C*, 2012, **116**, 20839.
7. P. Song, L.-P. Mei, A.-J. Wang, K.-M. Fang and J.-J. Feng, *Int. J. Hydrogen Energy*, 2016, **41**, 1645.
8. F. Ren, H. Wang, C. Zhai, M. Zhu, R. Yue, Y. Du, P. Yang, J. Xu and W. Lu, *ACS Appl. Mater. Interfaces*, 2014, **6**, 3607.
9. H. Li, H. Wu, Y. Zhai, X. Xu and Y. Jin, *ACS Catal.*, 2013, **3**, 2045.
10. A. Dutta and J. Ouyang, *ACS Catal.*, 2015, **5**, 1371.
11. K. Jiang, L. Bu, P. Wang, S. Guo and X. Huang, *ACS Appl. Mater. Interfaces*, 2015, **7**, 15061.
12. G. Li, L. Jiang, B. Zhang, Q. Jiang, D. s. Su and G. Sun, *Int. J. Hydrogen Energy*, 2013, **38**, 12767.
13. G. Yang, Y. Zhou, H.-B. Pan, C. Zhu, S. Fu, C. M. Wai, D. Du, J.-J. Zhu and Y. Lin, *Ultrason. Sonochem.*, 2016, **28**, 192.
14. C. Zhu, S. Guo and S. Dong, *J. Mater. Chem.*., 2012, **22**, 14851.
15. S. Mourdikoudis, M. Chirea, D. Zanaga, T. Altantzis, M. Mitrakas, S. Bals, L. M. Liz-Marzan, J. Perez-Juste and I. Pastoriza-Santos, *Nanoscale*, 2015, **7**, 8739.
16. E. E. Switzer, T. S. Olson, A. K. Datye, P. Atanassov, M. R. Hibbs and C. J. Cornelius, *Electrochim. Acta*, 2009, **54**, 989.
17. H. Qian, S. Chen, Y. Fu and X. Wang, *J. Power Sources*, 2015, **300**, 41.
18. T. Gunji, T. Tanabe, A. J. Jeevagan, S. Usui, T. Tsuda, S. Kaneko, G. Saravanan, H. Abe and F. Matsumoto, *J. Power Sources*, 2015, **273**, 990.
19. H. Wang, K. Jiang, Q. Chen, Z. Xie and W.-B. Cai, *Chem.commun.*, 2016, **52**, 374.